Distribution of Rovibrational Product States for the "Prompt" Reaction H + D_2($v = 0$, $j = 0-4$) → HD($v' = 1,2$, j') + D near 1.6 eV Collision Energy†

Brian D. Bean, Félix Fernández-Alonso, and Richard N. Zare*

Department of Chemistry, Stanford University, Stanford, California 94305

Received: July 31, 2000; In Final Form: December 5, 2000

We initiate the reaction H + D_2($v = 0$, $j = 0-4$) → HD ($v' = 1,2$, j') + D by photolyzing HBr in a 1:9 mixture of HBr and D_2 expanded into vacuum through a pulsed nozzle. The same laser pulse that initiates the reaction also detects the HD(v', j') product in a state-specific manner via 2 + 1 REMPI. From the product ion signals we extract HD(v', j') state distributions for the $v' = 1,2$ manifolds that are compared to existing quasiclassical trajectory (QCT) calculations at similar energies. We find good agreement between calculation and experiment for the distribution of rotational product states within each vibrational manifold. The line-of-centers nearly elastic specular scattering (LOCNESS) model predicts an inverted parabolic distribution of HD(v', j'_{red}) products where $j'_{red} = j'/j'_{max}$, and j'_{max} is the maximum predicted rotational state based on the angle-dependent reaction barrier of the H_3 potential energy surface and previously measured product scattering angle distributions. Additionally, this model is shown to hold for previous measurements of H + D_2 at a collision energy of 1.28 eV.

Introduction

The hydrogen-atom/hydrogen-molecule exchange reaction continues to fascinate those with an interest in fundamental elementary reactions because of its seeming theoretical simplicity. This reaction and its isotopic variations appear to be the system for which the most accurate calculations can be made. The history of the study of this reaction is full of examples of how our understanding of reaction dynamics has advanced and deepened, often being led by insightful theoretical treatments.[1,2] For example, it was for H + H_2 that the first scattering resonances in a chemical reaction were predicted.[3,4] Chief among early workers in this area was Kuppermann who together with his students gave an identification of resonance structures[5−7] and provided an interpretation of their physical meaning.[8,9] Twenty-five years after these structures were first predicted, these scattering resonances are finally being observed.[10,11]

Despite the successful isolation of resonances in the hydrogen exchange reaction, the H + H_2 reaction can be described by simple physical models to a good degree. In a series of recent works[12−14] we reported state-resolved differential cross sections for the reaction H + D_2($v = 0$, $j = 0-4$) → HD ($v' = 1,2$, j') + D near 1.6 eV collision energy. These studies were made under "prompt" conditions in which a single laser was used both to photolyze the precursor and to ionize the products. A line-of-centers nearly elastic specular scattering (LOCNESS) model[13] was put forth to explain the observed correlation between the peak of the product scattering distributions (differential cross sections—DCSs) and the product rotational state, j'. In this paper, we compliment the DCS studies by presenting the measured distribution of HD(v', j') product states (integral cross sections—ICSs) under the same reaction conditions. We also compare these measurements to previous QCT calculations by Blais and Truhlar[15] and show that by extending the LOCNESS model to include a linear opacity function we can reproduce the functional form of the experimental data.

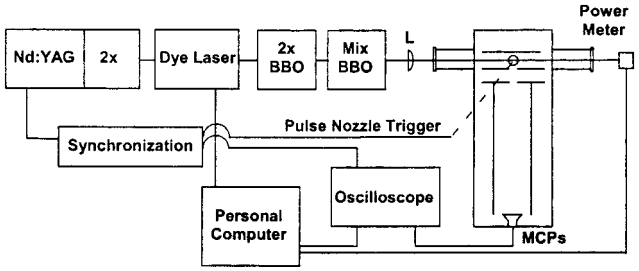

Figure 1. Experimental block diagram.

Experimental Section

The description of our experimental setup and the characterization of our reaction conditions have been presented elsewhere,[12] so we will outline only the main points. Hydrogen bromide (99.8% purity) is freeze−pump−thawed to remove H_2 contaminants and mixed in a 1:9 ratio with D_2 (99.8% purity) in a Teflon-lined stainless steel cylinder. The mixture enters a vacuum chamber through a pulsed nozzle with a typical pulse width of 600 μs and a backing pressure of 300 Torr. The vacuum chamber is differentially pumped and has baffled arms with fused silica windows for the laser beam entrance and exit. After the nozzle fires, a laser pulse (209−220 nm) enters the chamber where it photolyzes the HBr precursor and ionizes the HD(v', j') product of interest by 2 + 1 REMPI via the EF $^1\Sigma_g^+ - X\ ^1\Sigma_g^+$ transition.[16]

Up to 2 mJ of ultraviolet light can be created with the setup shown in Figure 1, consisting of an injection-seeded Nd:YAG-pumped dye laser whose output is tripled. The line width of the laser in the fundamental is 0.25 cm^{-1}, and the pulse duration is 7 ns. We employ a 1:3 Galilean telescope to expand the beam and a 600 mm suprasil lens to focus it into the chamber. We find that by expanding the beam before focusing, we produce

† Part of the special issue "Aron Kuppermann Festschrift".

* Author to whom correspondence should be addressed. E-mail: zare@stanford.edu.

10.1021/jp0027288 CCC: $20.00
Published on Web 02/14/2001

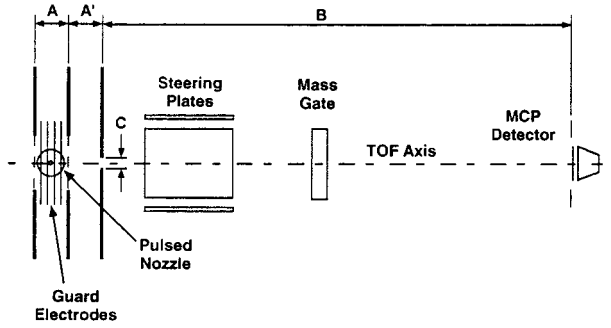

Figure 2. Bottom-view schematic diagram of time-of-flight spectrometer: $A = A' = 2.3$ cm; $B = 34.3$ cm; $C = 0.6$ cm. The potential drop across A is V and the potential drop across A' is $-cV$, where $c \sim 7.2$. The free-flight region (spanned by B) is kept at $-cV$.

a smaller, more homogeneous focal spot that ionizes HD more efficiently. As the laser pulse exits the chamber it is absorbed by a pyroelectric energy meter, and the reading is recorded concurrently with the ion signal.

The H + D_2 reaction and ionization of the HD(v', j') products take place in the extraction region of a Wiley−McLaren time-of-fight mass spectrometer.[17] The spectrometer consists of an extraction plate at $+V$, a repeller plate at $-V$, and a free-flight region at $-cV$, where $c = 7.2$ (Figure 2). A system of steering plates in the free-flight region allows us to adjust the trajectories of the HD(v', j') ions to strike the center of 25 mm microchannel plates (MCPs) that detect the ions. Because the line width of the laser is significantly smaller than the Doppler width of the HD(v', j') product molecules, it is necessary to scan the frequency of the laser over the transition (fwhm typically ~20 pm in dye laser fundamental).

The ion signal is collected by an oscilloscope and downloaded to a PC where it is integrated as a function of dye laser wavelength. We measured HD products for states $v' = 1$, $j' = 0-13$, and $v' = 2$, $j' = 0-8$. Each scan consists of 42 points taken in 2 pm steps. The raw ion signals were adjusted for fluctuations in power. Using a thin film polarizer and a half-wave plate, we reduced the power of the beam to determine the relationship between laser energy and signal intensity. The integrated area of the signal at the center of the transition was recorded as a function of power for HD($v' = 1, j' = 5$), HD($v' = 1, j' = 8$), and HD($v' = 2, j' = 3$) while complete profiles were taken for HD($v' = 2, j' = 1$) as a function of power. In all cases the power dependence was quadratic (exponent equal to 2.0 ± 0.2), implying that the ionization step in the 2 + 1 REMPI scheme and the photolysis of HBr were saturated. For the HD($v' = 2$) data, we scanned over each peak at least three times in the course of 2 days, and for the HD($v' = 1$) data we scanned over each peak at least six times in the course of 3 days.

Results and Discussion

Figure 3a shows a HD($v' = 1, j' = 9$) peak and Figure 3b shows a HD($v' = 2, j' = 4$) peak. Both peaks are typical of the signal-to-noise level in the experiment. The product distributions were constructed by adjusting the area of each peak to account for fluctuations in power and then averaging the measurements of each HD(v', j') state. It was not necessary to adjust the peaks for line strength as the experimental correction factors reported by Rinnen et al.[18] are unity (within error bars) for all of the HD(v', j') states measured. The average power adjusted ion signals are also reported in Table 1. The values reported in Table 1 were produced by normalizing the area of the $v' = 1$ and $v' = 2$ rotational distributions to the appropriate QCT calculations.

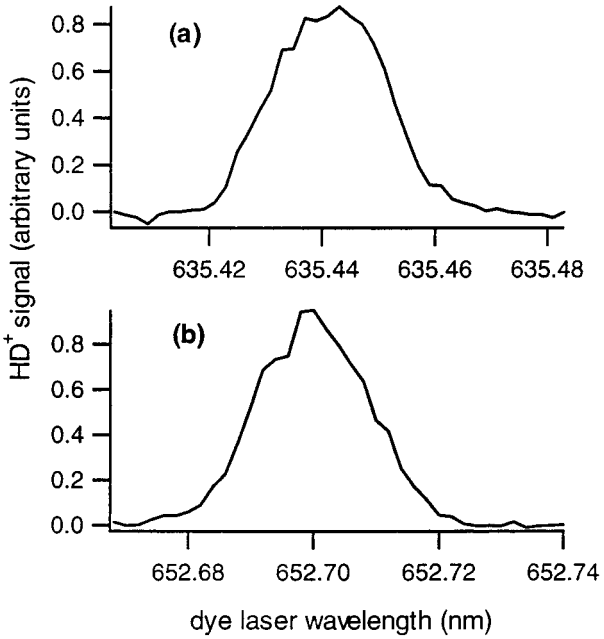

Figure 3. Typical 2 + 1 REMPI scan of the HD(v', j') product from the "prompt" reaction H + $D_2(v = 0, j = 0-4) \rightarrow HD(v', j') + D$ near 1.6 eV collision energy: (a) HD($v' = 1, j' = 9$); (b) HD($v' = 2, j' = 4$). Scans consist of 42 points in 2 pm steps. Signals were corrected for power fluctuations and averaged to produce the values in Table 1.

TABLE 1: HD(v', j') Product State Distributions for the Reaction H + $D_2(v = 0, j = 0-4) \rightarrow HD(v' = 1,2, j') + D$ near 1.6 eV Collision Energy

HD($v' = 1$) product rotational state	HD^+ ion signal in arbitrary units	HD($v' = 2$) product rotational state	HD^+ ion signal in arbitrary units
0	1.04(64)[a]	0	0.243(95)[a]
1	1.34(31)	1	0.67(35)
2	2.26(24)	2	1.18(17)
3	2.49(31)	3	1.15(16)
4	3.06(49)	4	1.232(55)
5	4.29(76)	5	1.15(26)
6	4.87(45)	6	0.78(25)
7	4.54(51)	7	0.372(38)
8	3.86(67)	8	0.29(16)
9	2.59(79)		
10	0.72(97)		
11	0.77(30)		
12	0.51(10)		
13	0.42(18)		

[a] Number in parentheses represents one standard deviation (67%) in the last digits, e.g., 3.06(49) means 3.06 ± 0.49.

The error reported in these measurements is the result of variation in the area under the 2 + 1 REMPI signals. When the laser power was unsteady, as for HD($v' = 2, j' = 1$), or when there were nonlinear crystal mode fluctuations, as for HD($v' = 1, j' = 10$), these errors were considerable (50% or greater).

Variation in Collision Energy. Because the probe laser is also responsible for the photolytic initiation of the reaction, the center-of-mass collision energy decreases as we tune the laser to detect higher rotational product states within a particular vibrational manifold. In addition, a complication arises from the existence of two accessible photolysis channels for HBr at these wavelengths. The "fast" channel corresponds to the production of ground-state Br($^2P_{3/2}$) atoms, and the "slow" to excited-state Br*($^2P_{1/2}$) atoms. Figure 4 shows the variation in center-of-mass collision energy for the H + D_2 "prompt" reaction as a function of the HD(v', j') product state detected. We have previously measured[12] that only 14 ± 3% of the H

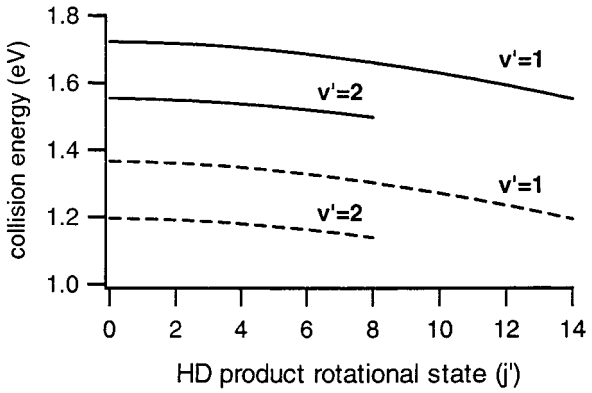

Figure 4. Variation of center-of-mass collision energy as a function of product state detected for the "prompt" reaction $H + D_2(v = 0, j = 0-4) \rightarrow HD(v', j') + D$ when HBr is the photolytic precursor. Solid line is the "fast channel" corresponding to the production of $Br(^2P_{3/2})$ and dashed line is the "slow channel" corresponding to the production of $Br^*(^2P_{1/2})$. Laser wavelengths vary from 209 to 217 nm for ($v' = 1$) and from 217 to 220 nm for ($v' = 2$).

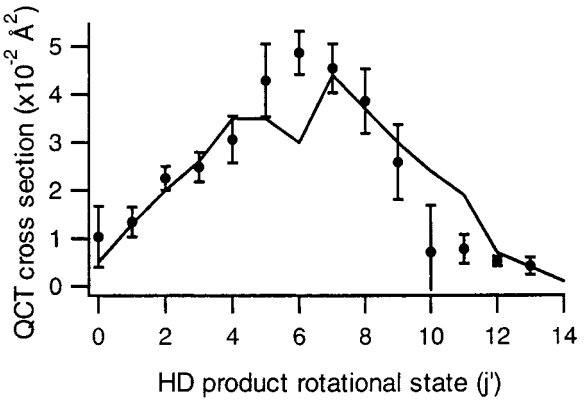

Figure 5. Experimentally measured $HD(v' = 1, j')$ product rotational state distribution (●) for the reaction $H + D_2(v = 0, j = 0-4) \rightarrow HD(v', j') + D$ near 1.6 eV collision energy and comparison to QCT calculations. Solid line is from the QCT calculations of Blais, N. C.; Truhlar, D. G. *Chem. Phys. Lett.* **1989**, *162*, 503. The experimental distribution has been normalized to the area under the QCT curve.

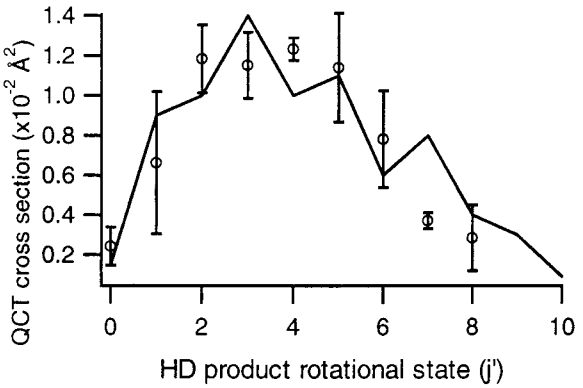

Figure 6. Same as Figure 5, but for $HD(v' = 2)$ products (○).

atoms produced under these conditions are from the slow (Br*) channel, in agreement with measurements of Regan et al.[19] In addition, because the cross sections for the slow channel reaction $H + D_2 \rightarrow HD(v' = 1,2, j') + D$ have been calculated[20,21] to be an order of magnitude smaller than the fast channel reactions,[15] we are justified in neglecting these contributions.

As can be seen in Figure 4, the collision energy of the $HD(v' = 1, j')$ distribution ranges from 1.72 to 1.57 eV while the $HD(v' = 2, j')$ distribution varies from 1.55 to 1.49 eV. In a previous paper,[12] we reported upper estimates for the rotational (90 K) and translational (45 K) temperatures of the HBr and D_2 precursors under identical reaction conditions. From these measurements we determined that the error in the center-of-mass collision energy is ±0.05 eV. Thus the spread in collision energy caused by the variation in photolysis wavelength represents the largest source of error when comparing experimental product state distributions to calculated integral cross sections.

Comparison to Quasiclassical Calculations. In 1989 Blais and Truhlar[15] (hereafter BT) used the QCT method to calculate ICSs for the reaction $H + D_2(v = 0, j) \rightarrow HD(v', j') + D$ at collision energies of 1.5, 1.6, 2.25, and 2.4 eV on the DMBE potential energy surface. These calculations were meant for comparison to experimental "prompt" state distribution measurements of the reaction $H + D_2(v = 0, j = 0-4) \rightarrow HD(v' = 0,1, j') + D$ by Rinnen et al.[18] for which HI was the photolytic precursor. Similar to HBr, HI also dissociates to yield $I(^2P_{3/2})$ and $I^*(^2P_{1/2})$ atoms, making it necessary to calculate ICSs at a number of collision energies to account for "fast" and "slow" H atoms corresponding to different spin−orbit states of the iodine atom. We are fortunate that the HI slow channel collision energies match the HBr fast channel collision energies for "prompt" reaction measurements of $H + D_2$.

Our results for $H + D_2(v = 0, j = 0-4) \rightarrow HD(v' = 1, j') + D$ at 1.72−1.57 ± 0.05 eV and $H + D_2(v = 0, j = 0-4) \rightarrow HD(v' = 2, j') + D$ at 1.52−1.49 ± 0.05 eV are compared to the results of BT at 1.6 and 1.5 eV in Figures 5 and 6. The agreement between experiment and theory is good with the exception of $HD(v' = 1, j' = 6)$, which exceeds the predicted value by nearly 50%. We hesitate to attribute this behavior to a genuine discrepancy in cross section for $HD(v' = 1, j' = 6)$ in light of our method of assigning scale to these numbers (i.e., normalizing total area to QCT area). Closer visual inspection, though, reveals that both measured rotational product state distributions are slightly cooler than the QCT calculations. This same behavior was observed when these calculations were compared to the results of Rinnen et al. [18] as originally intended. At other nearby collision energies (0.98−1.3 eV) this QCT method has been shown[21] to be in excellent agreement with rotational distributions as measured by coherent anti-Stokes Raman scattering (CARS),[22] but rotationally hotter than REMPI measurements.[23] We are not aware of similar QCT calculations made on the newer BKMP2 potential energy surface, but we would be surprised to see dramatic differences in light of past agreements between these surfaces at nearby energies.[24] In addition we are not aware of any quantum scattering calculations made for this system at these energies.

Comparison with the Predictions of the LOCNESS Model. In a recent paper,[13] we introduced the LOCNESS (line-of-centers nearly elastic specular scattering) model to explain the correlation between the cosine of the most probable scattering angle for a particular product state cos, θ_{mp} and j'^2, the square of the product state angular momentum for the reaction $H + D_2(v = 0, j = 0-4) \rightarrow HD(v', j') + D$ near 1.6 eV (Figure 4, ref 13). In a subsequent paper[14] we showed that this model provided a valid framework to explain the j'-dependence for the state-resolved, center-of-mass, angular distributions for the $v' = 2$ as well as the $v' = 1$ product manifolds.

The LOCNESS model contains elements of the optical model of Kwei and Herschbach,[25] the classical, kinematic model of Elsum and Gordon,[26] and the line-of-centers model.[27] These same elements were recently incorporated into a model by Truhins et al.[28] that used a Monte Carlo simulation to produce product state distributions for bimolecular reactions. These

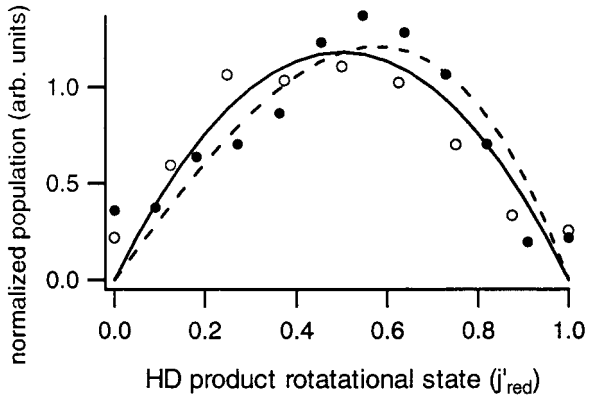

Figure 7. HD product rotational state distributions for the reaction H + $D_2(v = 0, j = 0-4) \rightarrow HD(v' = 1,2, j') + D$ near 1.6 eV plotted against j'_{red}, where $j'_{red} = j'/j'_{max}$ and j'_{max} is derived from the angle-dependent activation barrier of the LSTH PES. (●) HD($v' = 1$) manifold. (○) HD($v' = 2$) manifold. The solid line, $f(j'_{red}) = j'_{red}(1 - j'_{red})$, is the prediction of the LOCNESS model assuming a linear opacity function and the dashed line, $f(j'_{red}) = j'_{red}(1 - j'^2_{red})$, is the prediction of the angle-dependent line-of-centers model. Both model curves have been normalized to the area of the experimental vibrational manifolds.

simulations nicely reproduced rotational product state distributions for H + $D_2 \rightarrow HD(v' = 1,2) + D$ at 1.28 eV, as well as distributions for Cl + $H_2 \rightarrow$ HCl + H, and F + $I_2 \rightarrow$ IF + I. While not as robust as the model of Truhins et al., the LOCNESS model can predict a functional form that closely matches the HD(v', j') distributions reported here and at 1.28 eV without further computation (see below).

Starting with a simple optical model and assuming specular scattering, we can relate the scattering angle θ to a reduced impact parameter b_{red}, where $b_{red} = b/d$ and d is the hard-sphere diameter of the reactants and b the impact parameter:

$$\cos\theta = 2b_{red}^2 - 1 \tag{1}$$

In addition, borrowing from Elsum and Gordon's kinematic model we suggest the product rotational angular momentum j' is a linear function of the initial orbital angular momentum l:

$$j' = \alpha l \tag{2}$$

Using eqs 1 and 2, we can link j' to the scattering angle θ via l, where $l = \mu v b$. This results in the linear relationship between $\cos\theta_{mp}$ and j'^2 that we presented in previous works.

A line-of-centers analysis of reactive scattering in this system allowed us to predict expected maximum values of rotational product states for the $v' = 1,2$ manifolds near 1.6 eV collision energy. Using the experimentally measured angular distributions and the angle-dependent barrier to reaction of the LSTH potential energy surface[29-31] we determined the maximum rotational product state to be $j'_{max} = 11$ for $v' = 1$ (ref 13) and $j'_{max} = 8$ for $v' = 2$ (ref 14). Looking at the measured product state distribution in Figure 5, we see products in $j' = 12-13$ for the $v' = 1$ manifold, i.e., beyond $j_{max} = 11$. The presence of product states outside the LOCNESS model could be the result of reactions with rotationally excited D_2 [i.e., $D_2(v = 0, j = 4)$], where the internal energy of the D_2 has coupled with the collision energy to allow access to higher states. It is more likely, however, that the HD($v' = 1, j' = 12$) and HD($v' = 1, j' = 13$) states are the result of imperfect mapping between initial angular momentum and final rotational quantum number. By plotting the distribution of rotational products in the reduced variable $j'_{red} = j'/j'_{max}$, we can directly compare the two vibrational manifolds (Figure 7). It is striking to observe that both product states follow an inverted parabolic distribution peaking at $j'_{red} = 0.5$. The shape of this distribution can be approximated by a further extension of the LOCNESS model.

The cross section $\sigma(E)$ for the production of products into (v', j') at a given collision energy is simply the opacity function $P(E,b)$ integrated over all impact parameters. Going back to the relationship between the product rotational state and the impact parameter, $j' = \alpha\mu v b$, it follows from the quantization of j' that only a limited range of impact parameters can contribute to a particular (v', j') state. For a hard sphere reactant approaching another hard sphere this results in a dart-board-like target with annular rings of area $\sim 2\pi b db$.

On the basis of a line-of-centers argument we propose a linear opacity function for the preferentially collinear H + D_2 reaction of the form

$$P_{LONESS}(b) = c(1 - b_{red}) \tag{3}$$

Simply put, head-on ($b_{red} = 0$) collisions between reactants, where all of the translational energy is along the H−D−D axis, should be most reactive. As the H atom approaches with larger impact parameters, less energy will be available along the bond axis up to $b = d$ ($b_{red} = 1$), where no reaction should occur. This opacity function, taken over the quantized range of impact parameters for a particular j' state, will result in a j'-dependent cross section

$$\sigma_{LOCNESS}(j'_{red}) = c' j'_{red}(1 - j'_{red}) \tag{4}$$

This function has been normalized to the area of the HD ($v' = 1,2, j'_{red}$) distributions and is plotted (solid line) in Figure 7.

An alternative opacity function results from the angle-dependent line-of-centers (AD-LOC) model that accounts for the rotation of the D_2 molecule with respect to the incoming H atom.[27]

$$P_{AD-LOC}(b) = c(1 - b_{red}^2) \tag{5}$$

This opacity function results in a j'-dependent cross section

$$\sigma_{AD-LOC}(j'_{red}) = c' j'_{red}(1 - j'^2_{red}) \tag{6}$$

following the arguments above. This function has also been normalized and plotted in Figure 7. While both functions approximate the experimental points, the closer agreement between eq 4 and the j'_{red} distributions suggests that a linear opacity function is a reasonable approximation at these collision energies.

Extension to 1.28 eV. As a further test of the LOCNESS model, we have constructed $\cos\theta_{mp}$ vs j'^2 plots from state-to-state DCSs of the H + $D_2(v = j = 0) \rightarrow HD(v', j') + D$ reaction at 1.28 eV. The experimental points in Figure 8 are taken from the Rydberg atom time-of-flight measurements of Welge and co-workers.[32] Like the plots of $\cos\theta_{mp}$ vs j'^2 in previous works,[13,14] we again find linear relationships, suggesting that the LOCNESS model is valid over a range of energies. Additionally, we see that each vibrational manifold has a unique slope reflecting the change in hard-sphere diameter. Using the slopes of the lines in Figure 8, we can predict $j'_{max} = 11$ for the HD($v' = 0$) manifold, $j'_{max} = 9$ for the HD($v' = 1$) manifold, and $j'_{max} = 6$ for the HD($v' = 2$) manifold.

The predicted j'_{max} values can be used to produce reduced rotational product state distributions as described in the previous section. In Figure 9 we have normalized the ICS measurements

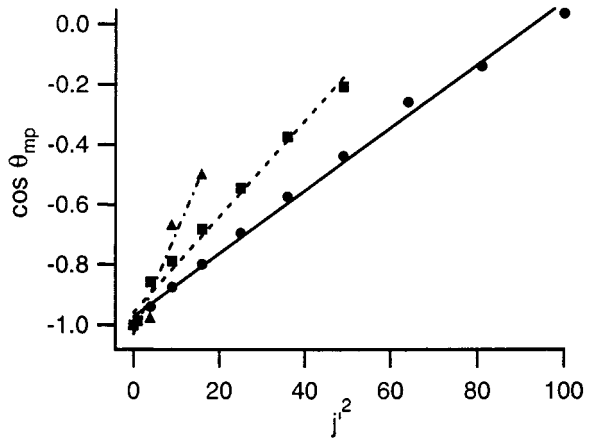

Figure 8. Correlation between the most probable scattering angle, θ_{mp}, and product rotational state, j', for the reaction H + $D_2(v = j = 0) \rightarrow$ HD(v', j') + D at 1.28 eV. (●) HD($v' = 0$) manifold. (■) HD($v' = 1$) manifold. (▲) HD($v = 2$) manifold. Data points are taken from Schnieder et al., *J. Chem. Phys.* **1997,** *107*, 6175. Lines are least-squares fits to data. (Solid line) HD($v' = 0$) manifold, slope = 0.0105. (Dashed line) HD($v' = 1$) manifold, slope = 0.0155. (Dot−dashed line) HD($v' = 2$) manifold, slope = 0.0338.

of H + $D_2(v = j = 0) \rightarrow$ HD(v', j') + D at 1.28 reported by Welge and co-workers[32] and plotted them versus $j'_{red} = j'/j'_{max}$. In addition, we have included the ICS measurements of H + $D_2(v = 0, j = 0-4) \rightarrow$ HD(v', j') + D at 1.28 eV by Zare and co-workers[33] who used a 2 + 1 REMPI detection method similar to the one described in this work. As can be seen in Figure 9, there is good agreement between the experimentally measured distributions and the predictions of the LOCNESS model (solid line).

There is a noticeable disagreement, however, between the two distributions in Figure 9a. This discordance is likely a reflection of the difficulty of measuring the population of HD($v' = 0$) products owing to reaction in the presence of HD impurities in the D_2 precursor. The 2 + 1 REMPI method used by Zare and co-workers cannot distinguish between contaminant and product HD($v' = 0$), whereas the Rydberg D-atoms detected in the Welge experiment, and used to build the ICS, are unique to a reaction. It is this ambiguity in REMPI detection for HD($v' = 0$, $j' = 0-4$) that discouraged us from attempting "prompt" reaction measurements of the HD($v' = 0$) products using HBr as a photolytic precursor.

Conclusions

We have measured the rovibrational distribution of product states for the reaction H + $D_2(v = 0, j = 0-4) \rightarrow$ HD($v' = 1,2, j'$) + D in the vicinity of 1.6 eV collision energy. We find good agreement within each vibrational manifold between the measured distributions and the quasiclassical calculations of Blais and Truhlar[15] on the DMBE PES. In addition, we showed that it is not necessary at these energies to account for the "slow" HBr photolysis channel when comparing experiments to calculations. Finally, the LOCNESS model is shown to reproduce the functional form of the integral cross sections when plotted as j'_{red}, where $j'_{red} = j'/j'_{max}$ and j'_{max} is inferred from the j' dependence of previously measured angular distributions[13,14] and the angle-dependent activation barrier of the LSTH PES. By examining previous measurements of DCSs[32] and ICSs[32,33] for H + D_2 at a 1.28 eV collision energy, we find that the LOCNESS model is not restricted to use only in the vicinity of 1.6 eV collision energy.

We are encouraged by the agreement between these experiments and calculations as well as the correlation between our rotational state distributions and those predicted by the LOCNESS model. The agreement with this simple model reinforces our classical "billiard-ball" intuition, even for this most fundamental reaction between light particles.

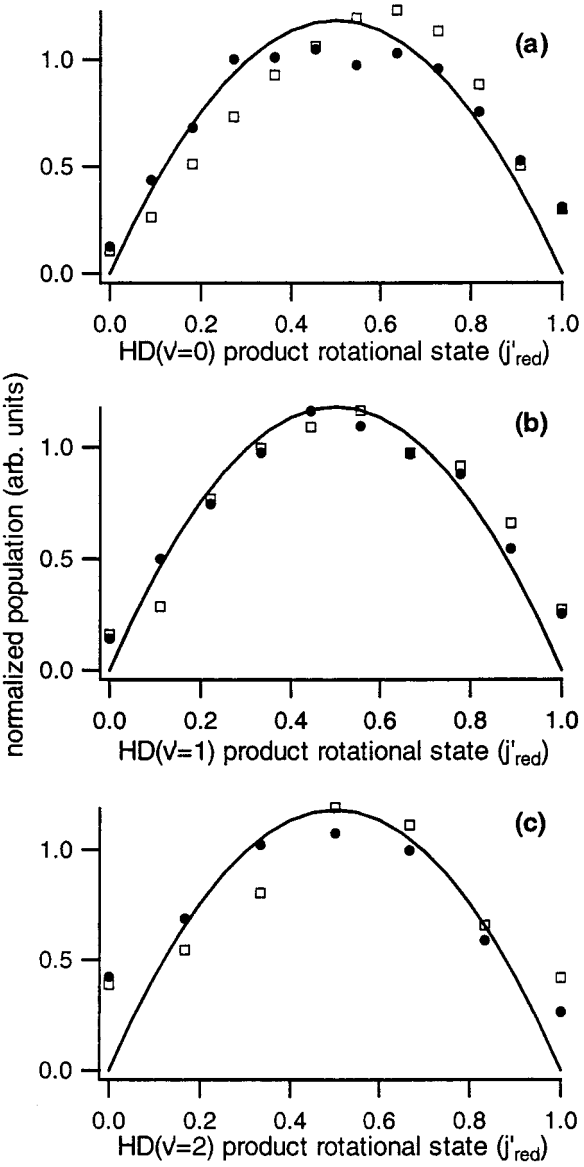

Figure 9. HD product rotational state distributions for the reaction H + $D_2(v = j = 0) \rightarrow$ HD(v', j') + D at 1.28 eV plotted against j'_{red}, where $j'_{red} = j'/j'_{max}$ and j'_{max} is derived from the slopes of Figure 8. (a) HD($v' = 0$) manifold, (b) HD($v' = 1$) manifold, (c) HD($v' = 2$) manifold. (●) Measurements of Rinnen et al. *J. Chem. Phys.* **1989**, *91*, 7514. (□) Measurements of Schnieder et al., *J. Chem. Phys.* **1997**, *107*, 6175. The solid line, $f(j'_{red}) = j'_{red}(1- j'_{red})$, is the prediction of the LOCNESS model that assumes a linear opacity function.

Acknowledgment. We thank J. D. Ayers and A. E. Pomerantz for useful discussions and critical proofreading. B.D.B. thanks Elf-Atochem for a graduate fellowship. The authors gratefully acknowledge the National Science Foundation for financial support under Grant No. CHE-93-22690 and CHE-99-00305.

References and Notes

(1) Miller, W. H. *Annu. Rev. Phys. Chem.* **1990**, *41*, 245.
(2) Truhlar, D. G.; Wyatt, R. E. *Annu. Rev. Phys. Chem.* **1976**, *27*, 1.
(3) Levine, R. D.; Wu, S.-F. *Chem. Phys. Lett.* **1971**, *11*, 557.
(4) Truhlar, D. G.; Kuppermann, A. *J. Chem. Phys.* **1972**, *56*, 2232.

(5) Schatz, G. C.; Kuppermann, A. *J. Chem. Phys.* **1973**, *59*, 964.
(6) Schatz, G. C.; Kuppermann, A. *Phys. Rev. Lett.* **1975**, *35*, 1266.
(7) Hipes, P. G.; Kuppermann, A. *Chem. Phys. Lett.* **1987**, *133*, 1.
(8) Cuccaro, S. A.; Hipes, P. G.; Kuppermann, A. *Chem. Phys. Lett.* **1989**, *157*, 440.
(9) Kuppermann, A. In *Potential Energy Surfaces and Dynamics Calculations*; Truhlar, D. G., Ed.; Plenum: New York, 1981; pp 375−420.
(10) Kendrick, B. K.; Jayasinghe, L.; Moser, S.; Auzinsh, M.; Shafer-Ray, N. *Phys. Rev. Lett.* **2000**, *84*, 4325.
(11) Fernández-Alonso, F.; Bean, B. D.; Ayers, J. D.; Pomerantz, A. E.; Zare, R. N.; Bañares, L.; Aoiz, F. J. *Angew. Chem., Int. Ed.* **2000**, 2748.
(12) Fernández-Alonso, F.; Bean, B. D.; Zare, R. N. *J. Chem. Phys.* **1999**, *111*, 1022.
(13) Fernández-Alonso, F.; Bean, B. D.; Zare, R. N. *J. Chem. Phys.* **1999**, *111*, 1035.
(14) Fernández-Alonso, F.; Bean, B. D.; Zare, R. N. *J. Chem. Phys.* **1999**, *111*, 2490.
(15) Blais, N. C.; Truhlar, D. G. *Chem. Phys. Lett.* **1989**, *162*, 503.
(16) Marinero, E. E.; Rettner, C. T.; Zare, R. N. *Phys. Rev. Lett.* **1982**, *48*, 1323.
(17) Wiley, W. C.; McLaren, I. H. *Rev. Sci. Inst.* **1955**, *26*, 1150.
(18) Rinnen, K.-D.; Kliner, D. A. V.; Blake, R. S.; Zare, R. N. *Chem. Phys. Lett.* **1988**, *153*, 371.
(19) Regan, P. M.; Langford, S. R.; Orr-Ewing, A. J.; Ashfold, M. N. R. *J. Chem. Phys.* **1999**, *110*, 281.
(20) Blais, N. C.; Truhlar, D. G. *Chem. Phys. Lett.* **1983**, *102*, 120.
(21) Blais, N. C.; Truhlar, D. G. *J. Chem. Phys.* **1985**, *83*, 2201.
(22) Gerrity, D. P.; Valentini, J. J. *J. Chem. Phys.* **1985**, *82*, 1323.
(23) Marinero, E. E.; Rettner, C. T.; Zare, R. N. *J. Chem. Phys.* **1984**, *80*, 4142.
(24) Aoiz, F. J.; Bañares, L.; Díez-Rojo, T.; Herrero, V. J.; Sáez-Rábanos, V. *J. Phys. Chem.* **1996**, *100*, 4071.
(25) Kwei, G. H.; Herschbach, D. R. *J. Phys. Chem.* **1979**, *83*, 1550.
(26) Elsum, I. R.; Gordon, R. G. *J. Chem. Phys.* **1982**, *76*, 3009.
(27) Smith, I. W. M. *J. Chem. Educ.* **1982**, *59*, 9.
(28) Truhins, K.; Marsh, R.; McCaffery, A. J.; Whiteley, T. W. J. *J. Chem. Phys.* **2000**, *112*, 5281.
(29) Siegbahn, P.; Liu, B. *J. Chem. Phys.* **1978**, *68*, 2457.
(30) Truhlar, D. G.; Horowitz, C. J. *J. Chem. Phys.* **1978**, *68*, 2466.
(31) Levine, R. D.; Bernstein, R. B. *Chem. Phys. Lett.* **1984**, *105*, 467.
(32) Schnieder, L.; Seekamp-Rahn, K.; Wrede, E.; Welge, K. H.; *J. Chem. Phys.* **1997**, *107*, 6175.
(33) Rinnen, K.-D.; Kliner, D. A. V.; Zare, R. N. *J. Chem. Phys.* **1989**, *91*, 7514.